A Unique Structural Pattern Shared by T-Cell-Activating and Abscess-Regulating Zwitterionic Polysaccharides†

Yong-Hoon Choi,‡ Michael H. Roehrl,§ Dennis L. Kasper,‡,|| and Julia Y. Wang*,‡

Channing Laboratory, Department of Medicine, Brigham and Women's Hospital, Department of Biological Chemistry and Molecular Pharmacology, and Department of Microbiology and Molecular Genetics, Harvard Medical School, Boston, Massachusetts 02115

Received July 25, 2002; Revised Manuscript Received September 23, 2002

ABSTRACT: In contrast to the conventional dogma that carbohydrates are poorly immunogenic T-cell-independent antigens, zwitterionic polysaccharides (ZPSs) can significantly stimulate T-cell proliferation and regulate abscess formation in bacterial infection. Despite their similar biological activities, ZPSs from various bacteria are greatly different in primary chemical compositions and building block linkages. To identify the common structural features that govern the peculiar immunologic activity of ZPSs, we have been determining three-dimensional structures of compositionally different ZPSs by NMR spectroscopy and molecular mechanics and dynamics calculations. We report here the conformation of type 1 capsular polysaccharide from the human pathogen *Streptococcus pneumoniae* (Sp1) to be a right-handed helix with repeated zwitterionically charged grooves. We also report the striking similarity between the structures of Sp1 and our previously determined PS A2 from *Bacteroides fragilis*. These results support our hypothesis that T-cell-activating ZPSs assume similar conformational and charge patterns that are recognized by specific receptors and that account for their common property as T-cell activators.

Carbohydrates have been traditionally regarded as incapable of eliciting T-cell responses and hence categorized as T-cell-independent antigens (*1*−*3*). More recently, however, it has been demonstrated that many bacterial capsular polysaccharides (PSs)[1] do, in fact, induce a variety of T-cell-specific responses such as cell proliferation, cytokine secretion, and regulation of antibody production (*4*−*9*). Of particular interest is a class of zwitterionic PSs (ZPSs) whose members have been discovered to be especially potent T-cell activators. ZPSs stimulate the proliferation of T cells in the presence of antigen-presenting cells, as demonstrated by in vitro T-cell proliferation and cytokine assays (*4*−*6*). Several bacterial ZPSs identified thus far, including PS A1, PS B, and PS A2 from *Bacteroides fragilis* and type 1 capsular polysaccharide from *Streptococcus pneumoniae* (Sp1), all activate T cells (*10*−*12*). They also can, in a context-dependent manner, induce or inhibit bacterial abscess formation, as has been demonstrated in rat models of intraabdominal abscesses (*5*, *13*). These findings strongly suggest that ZPSs are a novel class of T-cell antigens. Established T-cell antigens such as peptides, glycolipids, and protein superantigens have been instrumental for our fundamental understanding of immunology (*14*−*17*). An understanding of how ZPSs differ from other carbohydrates and exert their peculiar effects on T cells will provide important new insights into the structure−function relationship of carbohydrates and the immune system.

T-cell-activating ZPSs vary significantly in their monosaccharide compositions, linkages, and sequences. The only obvious common feature is their zwitterionic charge motif. Each ZPS carries a high density of positively charged amino and negatively charged carboxyl or phosphonate groups. The dual charge motif is generally rare among naturally occurring PSs but functionally critical for ZPSs (*4*, *5*, *12*). For example, chemical conversion of positively charged amines to neutral *N*-acetyl groups eliminates the activity of ZPSs (*8*, *18*). To explain why ZPSs comprising different carbohydrate sequences elicit similar T-cell responses, we hypothesized that the functionally common basis for the T-cell activity of ZPSs lies in overall spatial charge organization (*11*). We proposed that different ZPSs assume similar three-dimensional structures which may define a common scaffold for the presentation of charges and hence form a unique molecular pattern. To test this hypothesis, we have been determining the three-dimensional structures of various biologically active ZPSs. In our previous study, we elucidated the chemical structure and conformation of PS A2 from *B. fragilis* strain 638R (*11*). PS A2 forms an extended right-handed helix. Every helical turn defines a groove whose four edges are occupied by two pairs of zwitterionic charges. We report here the conformation of Sp1 from the human pathogen *S. pneumoniae* as

† This work was supported in part by National Institute of Allergy and Infectious Diseases (NIAID) Grant AI039576 to D.L.K.

* Corresponding author. Tel: +1-617-732-8585. Fax: +1-617-264-6845. E-mail: ywang@channing.harvard.edu.

‡ Channing Laboratory, Department of Medicine, Brigham and Women's Hospital, Harvard Medical School.

§ Department of Biological Chemistry and Molecular Pharmacology, Harvard Medical School.

|| Department of Microbiology and Molecular Genetics, Harvard Medical School.

[1] Abbreviations: MHC, major histocompatibility complex; PS, polysaccharide; RMSD, root mean squared deviation; rMD, restrained molecular dynamics; rSA, restrained simulated annealing; RU, repeating unit; Sp1, *Streptococcus pneumoniae* type 1 capsular polysaccharide; ZPS, zwitterionic polysaccharide.

10.1021/bi020491v CCC: $22.00
Published on Web 11/22/2002

determined by NMR spectroscopy and molecular mechanics and dynamics calculations. We also demonstrate the striking similarities between the solution conformations of Sp1 and PS A2.

MATERIALS AND METHODS

Purification of Sp1. Crude PS extracts from type 1 *S. pneumoniae* were purchased from the American Type Culture Collection (Atlanta, GA). A 20-mg sample of the crude material was dissolved in 1.5 mL of 2 M NaOH and heated to 80 °C for 3 h to degrade the contaminating ribitol phosphate teichoic acids (*19*, *20*). The mixture was then neutralized with 2 M HCl, dialyzed extensively against deionized water, and lyophilized. The product was then purified on a Sephacryl S300 column (Amersham Pharmacia Biotech, Piscataway, NJ) in phosphate-buffered saline (0.01 M phosphate, 0.15 M NaCl, pH 7.2) containing 0.05% azide. Fractions were monitored by a refractive index detector for carbohydrates and by a UV detector at 280 nm for contaminating proteins. Sp1 elutes close to the void volume of the column and has an average molecular mass of 100 kDa. Sp1 fractions were pooled, dialyzed extensively against deionized water, and lyophilized. Structural integrity and purity were verified by NMR analysis.

NMR Spectroscopy. All NMR spectra were obtained from a sample of 8 mg of purified Sp1, which was exchanged with D_2O once and redissolved in 0.7 mL of D_2O. NMR experiments were performed at 37 °C on a Varian Unity 500 instrument (Varian Inc., Palo Alto, CA). ^1H and ^{13}C chemical shifts were referenced externally to sodium 2,2-dimethyl-2-silapentane-5-sulfonate and CH_3I, respectively. Most spectra were obtained in the phase-sensitive TPPI mode with standard pulse sequences (*21*, *22*). $^1H-^1H$ TOCSY (*23*), DQF-COSY (*24*), and NOESY (*25*) spectra were recorded with spectral widths of 10 ppm in both dimensions. A spin-lock time of 80 ms was used for TOCSY. NOESY spectra were recorded with mixing times of 25, 50, 75, and 100 ms. $^3J_{H,H}$ couplings were measured from DQF-COSY and E.COSY to verify the chair configuration of monosaccharide constitutes (*26*). $^1H-^{13}C$ HMQC (*27*) and HMBC (*28*) were recorded with spectral widths of 100 and 180 ppm in the carbon dimension, respectively. HMQC spectra were recorded with and without ^{13}C decoupling during the acquisition to obtain $^1J_{CH}$ coupling constants.

Molecular Modeling. All molecular modeling calculations were performed using the INSIGHT II 2000 program (Accelrys, San Diego, CA) on an Octane workstation (Silicon Graphics, Mountain View, CA). The consistent valence force field (CVFF) with harmonic potential function and cross terms (*29*, *30*) was used for all calculations unless otherwise stated since it yields consistent results in grid searches of various disaccharide conformations in both charged and uncharged forms. No cutoff was imposed on the calculation of nonbonded interactions. All calculations were performed *in vacuo* with a distance-dependent dielectric constant ($\epsilon = 4r$) unless otherwise specified. Root mean squared deviations (RMSDs) of structures were calculated on the basis of non-hydrogen atoms. As partial fraying occurs in the less restricted termini, RMSDs were calculated separately for both the entire four repeating units (RUs) and also the central two RUs only.

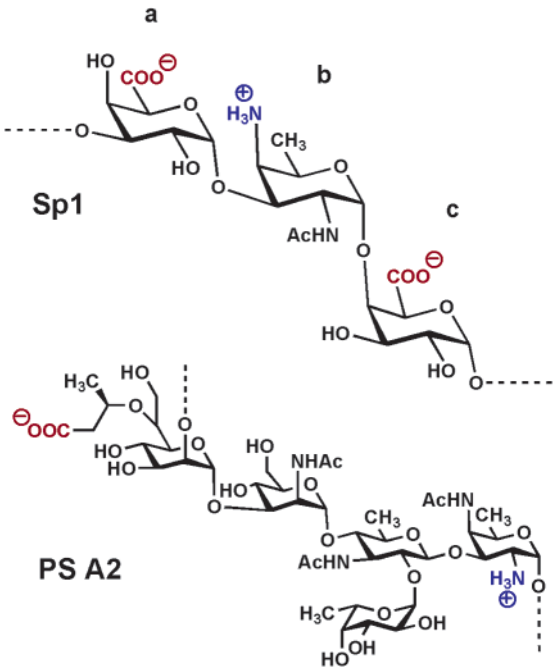

FIGURE 1: Chemical structures of Sp1 and PS A2.

Monosaccharide Model Building. The chemical structures of Sp1 and PS A2 are shown in Figure 1. Molecular models of the monosaccharide residues of Sp1 were built using the Biopolymer module of the INSIGHT II 2000 program. The free amino groups and the carboxyl groups in Sp1 were treated uncharged. An initial model of each monosaccharide was energy minimized by the steepest descent method until the maximum derivative was less than 1000 kcal·mol^{-1}·Å^{-1}, followed by the Polak−Ribiere conjugate gradient method until the maximum derivative was less than 10 kcal·mol^{-1}·Å^{-1} and a Newton minimization algorithm (BFGS) until the maximum derivative was less than 0.001 kcal·mol^{-1}·Å^{-1}.

Grid Search. The conformational space for each glycosidic linkage within one RU of Sp1 was assessed by systematic grid searches of the corresponding Φ_H and Ψ_H dihedral angles. Φ_H and Ψ_H are defined as H1−C1−O1−CX′ and C1−O1−CX′-HX′, respectively, where X′ refers to the glycosidic linkage site (*11*). $\Phi_H-\Psi_H$ potential energy maps were obtained by systematically rotating both dihedral angles from −180° to 180° in 10° increments. For every linkage, each of the 36^2 disaccharide structures was energy minimized as described above for the monosaccharides, while Φ_H and Ψ_H dihedral angles and the chair conformations of the carbohydrate rings were restrained (cosine restraints with $k = 1000$ kcal·mol^{-1}). The lowest energy $\Phi_H-\Psi_H$ dihedral angles in each potential energy map were selected to build the corresponding disaccharide, and the disaccharide was further energy minimized. This step of refinement was used to verify the accuracy and stability of the grid search.

The amino groups in residue **b** and the carboxyl groups in residues **a** and **c** were treated uncharged and charged in separate calculations to evaluate the charge contribution to overall structure. When treated charged, dielectric constants of $\epsilon = 4r$, 80, or $80r$ were used.

To investigate force field dependence of the grid search calculations, we also performed the same grid search calculations using the AMBER force field with Homans' additions for saccharides (*31*) which takes exoanomeric

effects into account and compared the results of the two different force fields.

Preliminary Structure Calculation. An initial molecular model of four RUs (containing 12 monosaccharides) of Sp1 was built with the preferred glycosidic dihedral angles obtained from the grid search calculations. Twenty-one interresidue NOE distance restraints for each RU were added to the initial model in the form of flat-bottomed energy terms with a proximal target value of 1.8 Å and distal target values of 3.3 Å for strong and 5.0 Å for weak NOE cross-peaks, respectively. Three interresidue NOE restraints, which originated from side chain methyl protons, were not included initially because they have minor influence on the overall structure calculation of Sp1. The force constants were set to 100 kcal·mol^{-1}·Å^{-2} with a scaling factor of 1. The molecular model was energy minimized to a final derivative of less than 0.001 kcal·mol^{-1}·Å^{-1} with NOE distance restraints to obtain a preliminary conformational model.

Iterative NOE Back-Calculation and Refinement of Distance Restraints. The NOE distance restraints were refined by an iterative process of NOE back-calculation and distance restraint adjustment. Simulated NOESY spectra were back-calculated from the preliminary conformational model of Sp1 (four RUs) using the program RELAX with a mixing time of 75 ms (*32*, *33*) and compared with the corresponding experimental NOESY spectrum. The refinement process was performed by one-by-one improvement of the simulated NOE peak which deviated the most from the corresponding experimental NOE peak at a given iteration. At each iteration, the problematic peak in the simulated NOESY spectrum was selected, and the corresponding distance restraint was adjusted to reduce the difference between the simulated and experimental volume of the corresponding peak without significantly affecting other peaks. If the volume of the problematic simulated peak was bigger than that of the experimental counterpart, larger values for proximal and distal distance restraints were applied. Conversely, if the volume of the problematic simulated peak was smaller than that of the experimental counterpart, smaller values for proximal and distal distance restraints were applied. At each iteration, several different combinations of proximal and distal target values for the problematic NOE peak were explored and resulting structures were subjected to NOE back-calculation. If necessary, push-apart distance restraints were introduced to remove simulated NOE peaks which were not present in the experimental spectrum (*34*). Once the problematic simulated NOE cross-peak had improved satisfactorily, the next discrepant peak was selected and refined again by the same method. Unlike in the preliminary conformational model, intraresidue NOE distance restraints were introduced if the problematic peak was an intraresidue NOE peak. The similarity between the simulated and experimental NOESY spectra was measured, first, by visual comparison, and, second, by the quality of the linear least-squares fit of simulated and experimental cross-peak intensities expressed as the regression coefficient, *R*. Visual comparison was important because it enabled comparison of overlapping peaks that could not be included in the regression calculation (*34*). This iterative process was repeated until no further improvement was noted.

Dependence on Initial Structures. To exclude structural bias and to investigate the effect of initial structure choice, five random linear conformations of Sp1 (four RUs) were also tested as initial structures for energy minimization with the refined NOE distance restraints. To randomize the conformation of Sp1, we performed a 50 ps molecular dynamics (MD) simulation at 1000 K. During the MD simulation, a distance restraint of 55−60 Å was applied between the two glycosidic oxygen atoms at each end of Sp1 to maintain a roughly linear conformation. Every 10 ps a snapshot was saved and used as an initial structure for energy minimization, imposing the refined NOE distance restraints. The five resulting structures were compared with the structure of Sp1 that had been obtained starting from the preferred glycosidic dihedral angles (see above).

Restrained Simulated Annealing. We performed a restrained simulated annealing (rSA) molecular dynamics calculation on Sp1 to refine the structure. The rSA was carried out with the refined NOE distance restraints. In the first high-temperature stage, the conformation of Sp1 was randomized during a 10 ps high-temperature MD simulation at 700 K. In the second cooling stage, the temperature was lowered from 700 to 300 K in decrements of 10 K per 5 ps. In the third low-temperature stage, a snapshot was taken at the end of the MD simulation at 300 K. Then the structure was randomized again by another stage of high-temperature MD simulation at 700 K. This scheme of high temperature−cooling−low temperature was performed for a total of five cycles. The five conformations taken at each 300 K MD step were fully energy minimized, imposing the refined NOE distance restraints until the maximum derivative was less than 0.001 kcal·mol^{-1}·Å^{-1}.

Restrained Molecular Dynamics. To further examine the conformational space and stability, we also performed a restrained molecular dynamics (rMD) simulation of Sp1 with the refined NOE distance restraints. The lowest energy structure obtained from the rSA was used as the starting geometry for the rMD simulation. A constant NVT molecular dynamics calculation was performed using the Verlet velocity algorithm with 1.0 fs time steps at 300 K. The system was equilibrated for 50 ps, and the production run was carried out for 1.0 ns. Temperature was controlled by velocity scaling in the equilibration phase and the Andersen algorithm in the production phase with a collision ratio of 1.0. Intermediate structures were saved every 1 ps for analysis.

RESULTS

NMR Studies. Sp1 from the type 1 capsule of *S. pneumoniae* is a linear polymer of trisaccharide repeating units, containing galacturonic acid (GalA, residues **a** and **c**) and 2-acetamido-4-amino-2,4,6-trideoxygalactose (Aat, residue **b**) with a sequence of →3)-α-D-GalA(**a**)-(1→3)-α-D-Aat(**b**)-(1→4)-α-D-GalA(**c**)-(1→ (Figure 1) (*13*, *35*). Each repeating unit of Sp1 contains one positively charged amine and two negatively charged carboxyl groups. To determine the three-dimensional structure of Sp1 by NMR, we obtained complete unambiguous assignments of the ^{1}H and ^{13}C resonances in the molecule. We used a combination of NMR experiments, including 1D ^{1}H (Figure 2) and 2D ^{1}H−^{1}H TOCSY, DQF-COSY, NOESY, ^{1}H−^{13}C HMQC with and without ^{13}C decoupling (Figure 2), and HMBC. The resonances in all spectra are well separated, and these experiments were sufficient for assignment (Table 1). Furthermore, the $^{1}J_{CH}$

Table 1: ^{1}H and ^{13}C Chemical Shift Assignments (in ppm) and $^{1}J_{CH}$ (in Hz) of Sp1

			1	2	3	4	5	6	NAc-CH_3
a	→3)-α-D-GalA-(1→	^{1}H	5.07	3.96	4.02	4.47	4.13		
		^{13}C	101.97	68.76	79.12	71.03	75.10		
		$^{1}J_{CH}$	173.0	150.4	145.0	150.4	144.0		
b	→3)-α-D-Sug-(1→	^{1}H	4.99	4.15	4.27	3.79	4.76	1.27	2.04
		^{13}C	101.19	50.51	76.18	55.92	65.75	18.18	25.19
		$^{1}J_{CH}$	176.9	129.3	146.8	149.5	149.5	127.9	130.0
c	→4)-α-D-GalA-(1→	^{1}H	5.22	3.93	4.08	4.39	4.61		
		^{13}C	99.85	70.83	71.63	82.26	73.90		
		$^{1}J_{CH}$	176.3	149.5	146.8	148.6	143.1		

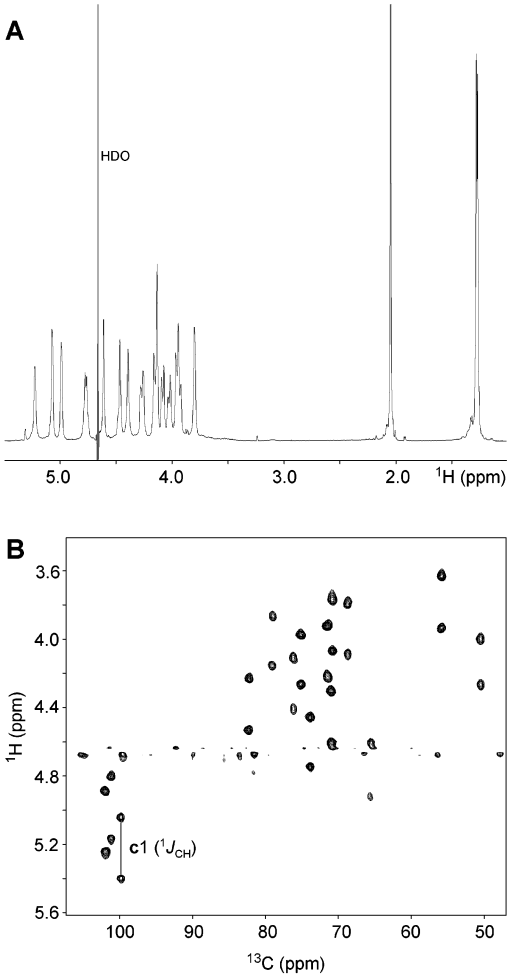

FIGURE 2: (A) ^{1}H spectrum of Sp1 recorded at 37 °C. (B) Partial $^{1}H-^{13}C$ HMQC spectrum of Sp1 (recorded without ^{13}C decoupling) from which $^{1}J_{CH}$ constants were obtained. The resonances and coupling arising from **c**1 are labeled.

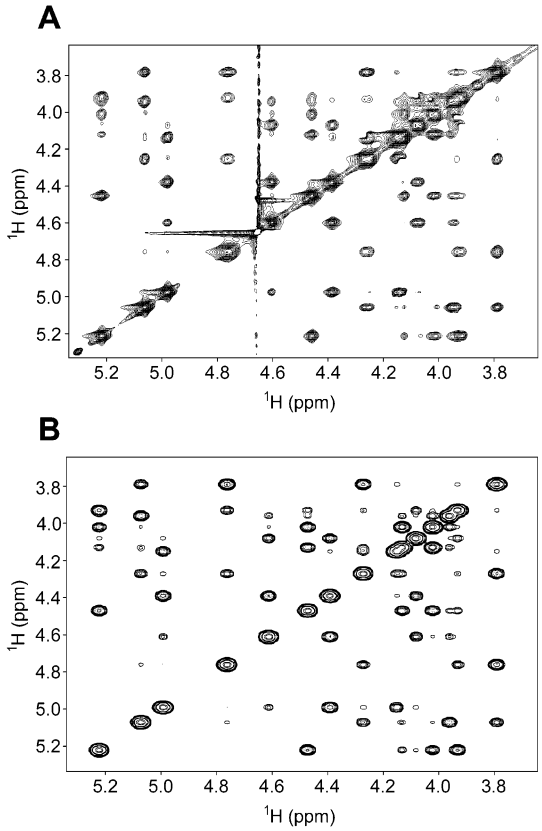

FIGURE 3: (A) NOESY spectrum of Sp1 with a mixing time of 75 ms. (B) Simulated NOESY spectrum of the lowest energy conformation of Sp1 from rSA.

(Table 1) couplings obtained from HMQC and $^{3}J_{HH}$ couplings from DQF-COSY confirmed the α anomeric configuration and the chair conformation of each monosaccharide constituent of Sp1.

To obtain distance constraints from NOEs, we acquired NOESY spectra of Sp1 at mixing times of 25, 50, 75, and 100 ms (Figure 3). NOE cross-peaks were assigned to protons within the same monosaccharide (intraresidue) or adjacent residues (interresidue). We detected a total of 27 intraresidue and 24 interresidue NOE cross-peaks per repeating unit. Cross-peak volumes were integrated for each mixing time, and NOE build-up curves were obtained. Most NOE intensities increased from 25 to 100 ms, except for two that increased from 25 to 75 ms, and decreased slightly at 100 ms. The NOE intensities at a mixing time of 75 ms, at which spin diffusion and zero-quantum coherence artifacts were minimal, were used to determine distance restraints (*36*). NOE cross-peak intensities were preliminarily classified as either strong or weak and interpreted as 1.8−3.3 Å and 1.8−5.0 Å distance intervals, respectively (*11*). Interresidue NOE-derived restraints were incorporated into the global structure calculation. Table 2 lists the interresidue NOEs used for structure calculation. A total of 4, 9, and 8 interresidue NOE distance restraints were used for **ab**, **bc**, and **ca** glycosidic linkages, respectively. Because 26 out of 27 intraresidue NOE distance restraints were already satisfied by the preliminary conformational model, intraresidue distance restraints were only introduced in the later refinement stages.

Conformational Preference. Poly- and oligosaccharides consist of monosaccharides joined by rotationally flexible glycosidic bonds. The global shape of an oligosaccharide depends mainly on the rotational flexibility of these glycosidic linkages, whereas the intrinsic flexibility of sugar rings is rather limited, and different orientations of the pendent

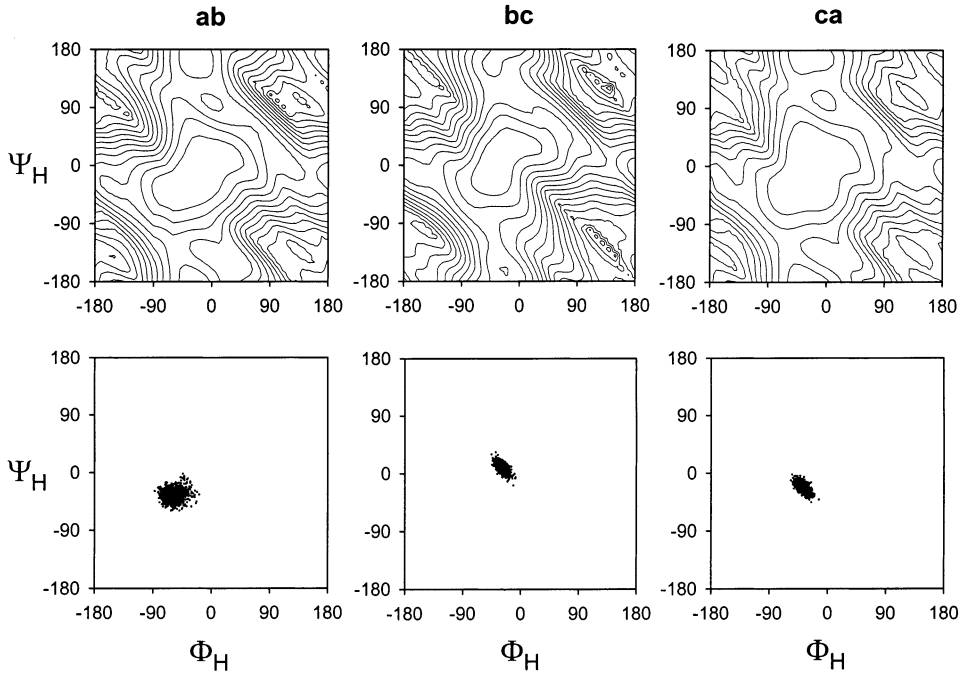

FIGURE 4: (Upper row) $\Phi_H-\Psi_H$ potential energy maps for the constituent glycosidic linkages (**ab**, **bc**, and **ca**) of Sp1. Isoenergetic contours are shown at 3 kcal/mol intervals above the global energy minimum for each map. (Lower row) Scatter plot of $\Phi_H-\Psi_H$ dihedral angles for the rMD trajectory.

Table 2: Interresidue NOE Volumes and Distance Restraints Used for the Calculation of Sp1 Structures

linkage	proton pair	NOE volume	distance restraint (Å)
ab	a1−b2	40.25	1.8−4.5
	a1−b3	114.91	1.8−3.3
	a1−b4	140.84	1.8−3.3
	a1−b5	23.73	4.6−5.0
bc	b1−c3	31.82	4.5−5.0
	b1−c4	220.45	1.8−3.3
	b1−c5	60.13	1.8−3.8
	b2−c4	42.20	1.8−4.6
	b3−c2	71.50	3.7−5.0
	b4−c2	56.84	1.8−4.0
	b5−c1	19.21	1.8−5.0
	b5−c2	131.76	1.8−3.3
	b5−c3	10.77	1.8−5.0
ca	c1−a3	110.95	1.8−3.3
	c1−a4	236.05	1.8−3.3
	c1−a5	54.38	1.8−5.0
	c2−a4	77.87	1.8−3.4
	c5−a2	70.56	1.8−3.2
	c5−a3	23.52	3.8−5.0
	c5−a4	9.84	1.8−5.0
	c5−a5	24.51	1.8−5.0

groups have minor influence on the conformational space of saccharides. To assess the conformational preferences of Sp1 due to the linkage and substitution patterns of the individual glycosidic components, we conducted systematic grid searches for every constituent glycosidic linkage. In this analysis, the Φ_H and Ψ_H dihedral angles of each glycosidic linkage were varied independently in 10° increments from −180° to 180°. The total energy was evaluated for each $\Phi_H-\Psi_H$ pair, and a $\Phi_H-\Psi_H$ potential energy map for each constituent disaccharide was obtained. Figure 4 shows the $\Phi_H-\Psi_H$ potential energy maps of the glycosidic linkages of Sp1. There is one global energy minimum for each disaccharide moiety. The low-energy regions within 3 kcal/mol above the global energy minima cover approximately 5−10% of the complete potential energy surface for each disaccharide. These preferred conformations were confirmed by starting from various dihedral angles for each glycosidic linkage and demonstrating convergence toward the global minima upon energy minimization. The resulting $\Phi_H-\Psi_H$ pairs of lowest energy were the following (linkages in parentheses): −50°, −35° (**ab**); −41°, 9° (**bc**); −41°, −35° (**ca**). Using the AMBER force field with Homans' additions for saccharides (*31*), we obtained virtually identical results for all linkages.

Charge Treatment. We treated the charged groups in Sp1 in four different ways. In the first case, the amino groups and the carboxyl groups were treated as neutral $-NH_2$ and −COOH with a dielectric constant of 4*r*. In the second through fourth cases, the amino and carboxyl groups were treated charged with dielectric constants of 4*r*, 80, or 80*r*, respectively. We performed grid search calculations for each case and then constructed corresponding structures of four RUs of Sp1. After energy minimization without NOE distance restraints, we assessed the final structures of each charge treatment by two standards. First, we investigated how many interresidue NOE distance restraints were already satisfied in each structure. The structure with neutral amino and carboxyl groups satisfied 19 out of 24 interresidue NOE distance restraints. The structures with charged amino and carboxyl groups and dielectric constants of 4*r*, 80, or 80*r* satisfied 15, 16, and 16 interresidue NOE distance restraints, respectively. Second, we investigated the consistency of glycosidic dihedral angles in the central two RUs of Sp1. The structure with neutral amino and carboxyl groups and a dielectric constant of 4*r* showed the highest consistency in its glycosidic dihedral angles. Therefore, we selected uncharged amino and carboxyl groups with a dielectric constant of 4*r* for the remainder of our modeling calculations.

Preliminary Conformational Model of Sp1. We investigated the preferred conformations of four RUs of Sp1. The

analysis of one repeating unit in isolation is generally too short to give an overall accurate representation of the conformation of a polysaccharide (*11*). Structure calculations that include several RUs improve local precision and accuracy and allow for the analysis of the central portion which is little disturbed by artifactual fraying of the less restrained termini. Preliminary conformational models of Sp1 fragments were computed by energy minimization with interresidue NOE distance restraints. The criteria for the preliminary classification of strong and weak peaks were obtained from the linear plot of the peak volumes vs $1/r^{-6}$ (r, distance between hydrogen atoms) for intraresidue NOE peaks. An initial model of Sp1 was built using the favorable $\Phi_H-\Psi_H$ dihedral angles obtained from the grid search and then fully energy minimized with NOE-derived distance restraints. The $\Phi_H-\Psi_H$ dihedral angles of the resulting conformation, averaged over the central two RUs, were the following: −64.5°, −32.0° (**ab**); −30.6°, 17.8° (**bc**); −62.8°, −22.3° (**ca**). All of these $\Phi_H-\Psi_H$ dihedral angles belong to the corresponding lowest energy regions in the $\Phi_H-\Psi_H$ potential energy maps, and all interresidue distance restraints were satisfied in this conformation after energy minimization. We also explored a slightly different approach, in which the initial models were fully energy minimized first without and then with NOE distance restraints. The RMSD between these two structures is only 0.6 Å for the entire four RUs and 0.4 Å for the central two RUs, indicating that the two energy minimization schemes yielded practically the same results. We used the former method for the rest of the structure calculations.

Structure Refinement and NOE Back-Calculation. The structure of Sp1 was refined via the iterative process of NOE back-calculation and NOE distance restraint adjustment. Ultimately, we incorporated 21 interresidue, 4 intraresidue, and 6 push-apart interresidue NOE distance restraints per RU into the structure calculation. The final set of refined NOE distance restraints was obtained after 54 cycles of this iterative refinement process and is listed in Table 2. The regression coefficient, R, of the scatter plot of experimental vs simulated interresidue NOE peak intensities improved from 0.91 to 0.95 when overlapping peaks were not considered. The improved R value indicates a good correlation between the experimental and simulated NOE data. Although it was difficult to accurately measure the volumes of a few overlapping cross-peaks near the diagonal in the experimental NOESY spectra, their correlation with the simulated NOE cross-peaks was very good. After the final round of structure refinement, the back-calculated NOESY spectra from the refined structure compare very well with the experimental spectra. As shown in Figure 3, the experimental NOESY and the simulated spectra from the lowest energy conformation of Sp1 are nearly identical.

Initial Structure Dependence. We also tested five random linear conformations of four RUs to investigate the importance of initial structure on the final results. When carbohydrate rings were restrained to standard $^4C_1$ chair conformations, all resulting conformations were within RMSD values of 1.8 Å for the entire four RUs and 0.9 Å for the central two RUs with respect to the energy-minimized conformation that had been obtained starting from the preferred glycosidic dihedral angles. Regardless of initial conditions, all resulting conformations converge to a family of closely related structures (Figure 5). On the basis of the high similarity of final Sp1 structures obtained from different initial structures, we conclude that there is no initial structure dependence. This result indicates that our molecular modeling procedure produces a unique structure.

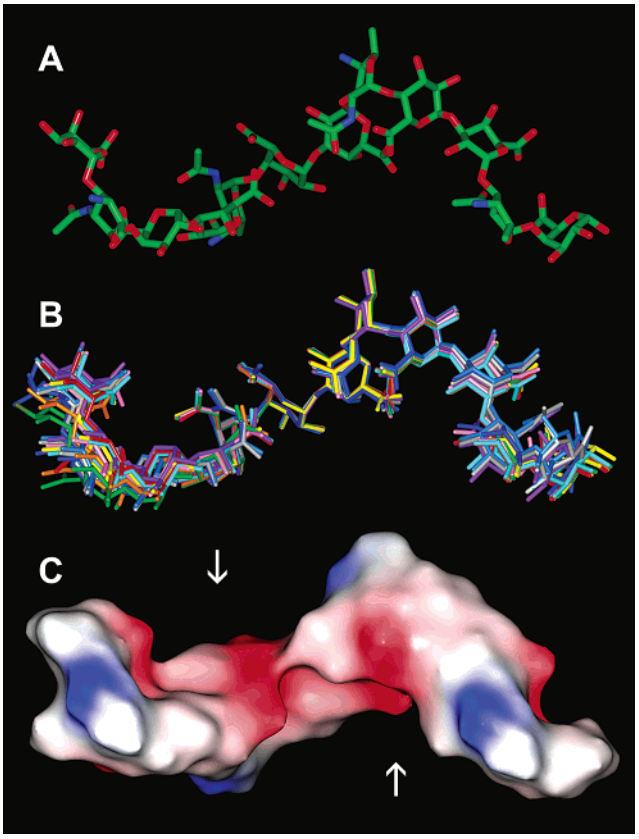

FIGURE 5: (A) Lowest energy conformation of Sp1 (four RUs) from rSA. Carbon, oxygen, and nitrogen atoms are colored green, red, and blue, respectively. (B) Superposition of 10 energy-minimized Sp1 conformations calculated with refined NOE distance restraints: four from rSA (red, cyan, yellow, orange), five from energy minimizations starting from random initial conformations (blue, violet, sky blue, gray, pink), and one from energy minimization starting from the preferred glycosidic dihedral angles (green). (C) Electrostatic surface representation of the lowest energy conformation of Sp1 from rSA. The orientation is identical to that in (A) and (B). Positive charges are colored blue and negative charges are colored red. Surface rendering and qualitative Poisson−Boltzmann electrostatic calculations were carried out with SPOCK (*39*). Note the two large grooves denoted by arrows and the alternating zwitterionic charge pattern.

Restrained Simulated Annealing. To further refine the structure, we conducted five rounds of rSA from 700 to 300 K. The conformations of Sp1 (4 RUs) were fully energy minimized at the end of each cycle. Out of the five resulting conformations, one was discarded because it had a carbohydrate ring which was distorted from the normal $^4C_1$ chair configuration. The other four conformations from rSA were compared with the lowest energy structure obtained by energy minimization with NOE distance restraints as described above. All five conformations form a family of closely related structures and are within RMSD values of 0.7 Å for the entire four RUs and 0.6 Å for the central two RUs. Figure 5 shows the lowest energy conformation of Sp1 and the overlay of structures from energy minimizations and rSA calculations with refined NOE distance restraints.

Restrained Molecular Dynamics Simulation. The stability of the Sp1 structure was investigated by rMD simulation with NOE distance restraints. The $\Phi_H-\Psi_H$ dihedral angles in the rMD trajectory exhibit stable conformational equilibria for all linkages within the lowest energy regions of their $\Phi_H-\Psi_H$ potential energy maps (Figure 4) even though fewer NOE restraints (4) are incorporated for the **ab** linkage than for **bc** (9) or **ca** (8) linkages. The time-averaged values of $\Phi_H-\Psi_H$ pairs ($\pm$ standard deviations) for the central two RUs were the following (linkages in parentheses): $-61.8 \pm 10.2°$, $-36.4 \pm 8.9°$ (**ab**); $-28.2 \pm 5.8°$, $8.2 \pm 7.0°$ (**bc**); $-37.6 \pm 6.3°$, $-22.4 \pm 6.5°$ (**ca**).

The RMSDs between structures of the rMD trajectory are on the order of 2 Å for the entire four RUs and 1 Å for the central two RUs. The successful convergence to a common conformation indicates the precision of the rMD simulation. The most significant differences arise at the terminal regions and can be attributed to end fraying.

DISCUSSION

Existence of a Unique Structure. Our structural calculations result in a unique, well-defined conformation for Sp1 which simultaneously satisfies all NOE data. Whenever NMR-based methods of structural elucidation are applied to saccharides, where multiple conformations may exist and contribute to the NMR data, we have to consider the possibility that a physically unrealistic or averaged conformation might be obtained (*37*, *38*). The following arguments, however, make this possibility seem unlikely. Each glycosidic linkage within Sp1 possesses only a single major low energy well in its $\Phi_H-\Psi_H$ potential energy space, and all glycosidic dihedral angles in structures that were calculated with NOE distance restraints fall within their corresponding low-energy wells. The consistency of glycosidic dihedral angles, regardless of the incorporation of NOE distance restraints, indicates that, for each linkage, an energetically stable linkage can exist in a single well-defined conformation that satisfies NOE data. Although it is premature to conclude that Sp1 necessarily adopts one rigid single conformation, our structure is, at least, a representative average structure of Sp1 which fits the NOE data excellently. Furthermore, the fact that only one set of chemical shift resonances is observed for Sp1 in NMR experiments argues against the coexistence of two or more fundamentally different Sp1 structures in solution. Functional arguments for the existence of well-defined structural features of Sp1 are given further down when comparing the structure with that of another T-cell-activating ZPS, PS A2.

3D Structure of Sp1. The overall conformation of Sp1 is an extended right-handed helix with eight residues per turn and a pitch of 20 Å (Figure 5). The molecular surface is covered with a high density of both positive and negative charges, as illustrated by the electrostatic surface representation (Figure 5). Within each RU, the two carboxyl groups (residues **a** and **c**) are spaced closely (4.6 Å) and positioned on one side of the helix, whereas the amino group (residue **b**) is positioned on the other side. The distances between charges are as follows: carboxyl group (residue **a**)−7.3 Å−amine (residue **b**)−7.4 Å−carboxyl group (residue **c**)−9.3 Å−carboxyl group (residue **a**). The distances between the amine and two carboxyl groups in one RU are approximately equal, whereas the carboxyl groups from different RUs are farther apart. Although one RU has two negative charges and one positive charge, the overall pattern of charge distribution can be described as an arrangement of alternating positive and negative charges along the polymer chain due to the proximity of two negative charges on residues **a** and **c**. If the two carboxyl groups in one RU are considered jointly (center of mass), the distances between charges are as followa: positive charge−7.0 Å−combined negative charge−8.5 Å−positive charge. The positive and negative charges are located approximately in analogous positions along the polymer chain but face opposite directions.

Like the previously determined structure of PS A2 (*11*), the helix of Sp1 is characterized by repeated charged grooves (Figure 5). Roughly one helical turn defines one groove on one side. One groove can be represented as $\mathbf{a}_{x-1}-\mathbf{b}_x-\mathbf{c}_x-\mathbf{a}_{x+1}-\mathbf{b}_{x+1}-\mathbf{c}_{x+1}-\mathbf{a}_{x+2}-\mathbf{b}_{x+2}-\mathbf{c}_{x+2}$, where x denotes a given RU. The grooves are approximately 14 Å wide, 10 Å long, and 5 Å deep. The size of the grooves of Sp1 is comparable to that of PS A2 (10 Å × 10 Å × 5 Å) (*11*). The positive charges on residues $\mathbf{b}_x$ and $\mathbf{b}_{x+2}$ are located along the lateral groove wall, while the positive charge on residue $\mathbf{b}_{x+1}$ is a part of another groove located on the other side of the helix. The negative charges on residues $\mathbf{c}_x$, $\mathbf{a}_{x+1}$, $\mathbf{c}_{x+1}$, and $\mathbf{a}_{x+2}$ occupy the floor and two sides of the groove and are shared by adjacent grooves.

Superposition of Sp1 and PS A2 Structures. In our previous study, we showed that PS A2 forms an extended right-handed helix with positive and negative charges exposed on the outer surface in a regularly spaced pattern (*11*). The chemical structure of PS A2 is completely different from that of Sp1 (Figure 1). While Sp1 is composed of galacturonic acid and 2-acetamido-4-amino-2,4,6-trideoxygalactose, PS A2 contains fucose, mannoheptose, 2-amino-4-acetamido-2,4,6-trideoxygalactose, 3-acetamido-3,6-dideoxyglucose, and 3-hydroxybutanoic acid (*11*). Despite the drastic differences in their primary structures, Sp1 and PS A2 assume remarkably similar three-dimensional conformations (Figure 6). For this comparison, a conformational model of Sp1 was constructed on the basis of the average glycosidic dihedral angles from the central two RUs of the lowest energy conformation from rSA. The glycosidic oxygen atoms of Sp1 can be superimposed onto the glycosidic oxygen atoms of PS A2 with an RMSD of 1.6 Å, revealing that these two ZPSs have essentially the same backbone conformation. In addition, the spatial arrangements of the amines in the two polysaccharides display a very similar pattern (Figure 6). In both molecules, the amines point outward and are arranged in a zigzag fashion. The average distance between adjacent amines in Sp1 is 14.6 Å, which is very similar to that of PS A2 (15.5 Å). Even when Sp1 and PS A2 are superimposed solely on the basis of their amino groups, the overlap of their backbone structures is still evident (Figure 6).

ZPSs possess exceptional immunological activities in that they are recognizable by both B and T lymphocytes and thus have the ability to modulate the dual arms of the host immune system. ZPSs are a novel class of T-cell antigens and revise the conventional dogma that carbohydrates are T-cell-independent antigens. At present, the mechanism by which ZPSs are recognized by T cells is not known. The conformational similarity between PS A2 and Sp1 strongly supports our hypothesis that a similar three-dimensional structure of compositionally dissimilar ZPSs accounts for their common

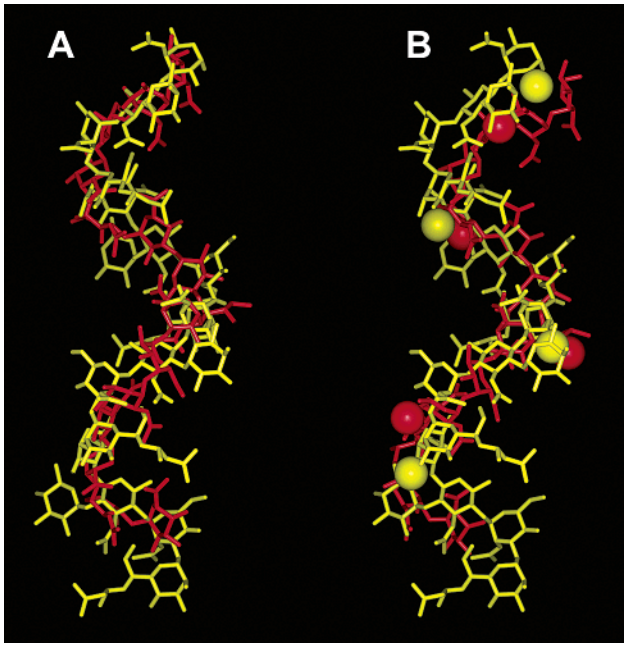

FIGURE 6: (A) Structures of Sp1 (red) and PS A2 (yellow) superimposed on the basis of their glycosidic oxygen atoms with an RMSD of 1.6 Å. (B) Structures of Sp1 (red) and PS A2 (yellow) superimposed on the basis of their amino groups. Red and yellow dots represent positive charges from Sp1 and PS A2, respectively. Sp1 and PS A2 display a similar zigzag positive charge pattern with roughly equidistant charge separation of 15 Å.

properties as T-cell activators. The common positive charge pattern underlines the importance of the amines for the biological function of ZPSs. The two three-dimensional ZPS structures that are now solved provide exciting biochemical probes for understanding how T cells recognize carbohydrates. The understanding of the molecular mechanism of ZPS-mediated T-cell responses has potentially profound implications for the basic science of immunology as well as the practical use of carbohydrates as a novel class of immunomodulators.

REFERENCES

1. Nahm, M. H., Apicella, M. A., and Briles, D. E. (1999) Immunity to Extracellular Bacteria, in *Fundamental Immunology* (Paul, W. E., Ed.) pp 1373−1386, Lippincott-Raven Publishers, Philadelphia, PA.
2. Rubin, L. G. (2000) *Pediatr. Clin. North Am. 47*, 269−285.
3. Jedrzejas, M. J. (2001) *Microbiol. Mol. Biol. Rev. 65*, 187−207.
4. Tzianabos, A. O., Wang, J. Y., and Lee, J. C. (2001) *Proc. Natl. Acad. Sci. U.S.A. 98*, 9365−9370.
5. Tzianabos, A. O., Finberg, R. W., Wang, Y., Chan, M., Onderdonk, A. B., Jennings, H. J., and Kasper, D. L. (2000) *J. Biol. Chem. 275*, 6733−6740.
6. Brubaker, J. O., Li, Q., Tzianabos, A. O., Kasper, D. L., and Finberg, R. W. (1999) *J. Immunol. 162*, 2235−2242.
7. Baker, P. J. (1992) *J. Infect. Dis. 165* (Suppl. 1), S44−S48.
8. Zirk, N. M., Hashmi, S. F., and Ziegler, H. K. (1999) *Infect. Immun. 67*, 319−326.
9. Kalka-Moll, W. M., Wang, Y., Comstock, L. E., Gonzalez, S. E., Tzianabos, A. O., and Kasper, D. L. (2001) *Infect. Immun. 69*, 2339−2344.
10. Baumann, H., Tzianabos, A. O., Brisson, J. R., Kasper, D. L., and Jennings, H. J. (1992) *Biochemistry 31*, 4081−4089.
11. Wang, Y., Kalka-Moll, W. M., Roehrl, M. H., and Kasper D. L. (2000) *Proc. Natl. Acad. Sci. U.S.A. 97*, 13478−13483.
12. Tzianabos, A. O., Onderdonk, A. B., Rosner, B., Cisneros, R. L., and Kasper, D. L. (1993) *Science 262*, 416−419.
13. Lindberg, B., Lindqvist, B., Lonngren, J., and Powell, D. A. (1980) *Carbohydr. Res. 78*, 111−117.
14. Reinherz, E. L., Tan, K., Tang, L., Kern, P., Liu, J., Xiong, Y., Hussey, R. E., Smolyar, A., Hare, B., Zhang, R., Joachimiak, A., Chang, H. C., Wagner, G., and Wang, J. (1999) *Science 286*, 1913−1921.
15. Hennecke, J. and Wiley, D. C. (2000) *Cell 104*, 1−4.
16. Moody, D. B., Ulrichs, T., Muhlecker, W., Young, D. C., Gurcha, S. S., Grant, E., Rosat, J. P., Brenner, M. B., Costello, C. E., Besra, G. S., and Porcelli, S. A. (2000) *Nature 404*, 884−888.
17. Li, Y., Li, H., Dimasi, N., McCormick, J. K., Martin, R., Schuck, P., Schlievert, P. M., and Mariuzza, R. A. (2001) *Immunity 14*, 93−104.
18. Bondada, S., Wu, H., Robertson, D. A., and Chelvarajan, R. L. (2000) *Vaccine 19*, 557−565.
19. Jennings, H. J., Lugowski, C., and Young, N. M. (1980) *Biochemistry 19*, 4712−4719.
20. van Dam, J. E. G., Fleer, A., and Snippe, H. (1990) *Antonie van Leewenhoek 58*, 1−47.
21. Sanders, J. K. M., and Hunter, B. K. (1993) *Modern NMR Spectroscopy*, Oxford University Press, New York.
22. Braun, S., Kalinowski, H.-O., and Berger, S. (1998) *150 and More Basic NMR Experiments*, Wiley-VCH, New York.
23. Bax, A., and Davis, D. G. (1985) *J. Magn. Reson. 65*, 355−360.
24. Piantini, U., Sørensen, O. W., and Ernst, R. R. (1982) *J. Am. Chem. Soc. 104*, 6800−6801.
25. Bodenhausen, G., Kogler, H., and Ernst, R. R. (1984) *J. Magn. Reson. 58*, 370−388.
26. Griesinger, C., Sørensen, O. W., and Ernst, R. R. (1987) *J. Magn. Reson. 75*, 474−492.
27. Bax, A., and Subramanian, S. (1986) *J. Magn. Reson. 67*, 565−569.
28. Bax, A., and Summers, M. F. (1986) *J. Am. Chem. Soc. 108*, 2093−2094.
29. Accelrys (1997) *Discover Forcefield Simulations User Guide*, Accelrys, San Diego.
30. Hagler, A. T., Lifson, P., and Dauber, P. (1979) *J. Am. Chem. Soc. 101*, 5122−5130.
31. Homans, S. W. (1990) *Biochemistry 29*, 9110−9118.
32. Goler, A., and Kalbitzer, H. R. (1997) *J. Magn. Reson. 124*, 177−188.
33. Goler, A., Gronwald, W., Neidig, K. P., and Kalbitzer, H. R. (1999) *J. Magn. Reson. 137*, 39−45.
34. Calafat, A. M., Won, H., and Marzilli, L. G. (1997) *J. Am. Chem. Soc. 119*, 3656−3664.
35. Bock, K., Lonn, H., and Peters, T. (1990) *Carbohydr. Res. 198*, 375−380.
36. Wüthrich, K. (1986) *NMR of Proteins and Nucleic Acids*, John Wiley & Sons, New York.
37. Cumming, D. A., and Carver, J. P. (1987) *Biochemstry 26*, 6664−6676.
38. Mulloy, B., and Forster M. J. (2000) *Glycobiology 10*, 1147−1156.
39. Christopher, J. A. (1998) *SPOCK: The Structural Properties Observation and Calculation Kit*, Center for Macromolecular Design, Texas A&M University, College Station, TX.

BI020491V